Nanotechnology

DOI: 10.1002/ange.201002295

Nanoparticle Supracrystals and Layered Supracrystals as Chemical Amplifiers**

*Bartlomiej Kowalczyk, David A. Walker, Siowling Soh, and Bartosz A. Grzybowski**

One of the main applications of metal nanoparticles (NPs) is in the detection of biologically important[1] or toxic substances,[2] usually by the spectral or surface plasmon resonance (SPR) changes[3] accompanying particle aggregation[4] or dispersion[2c,5] in the presence of an analyte. With the exception of highly sensitive DNA-based methods,[6] however, most reported colorimetric detection schemes require large excesses of analyte molecules per one NP (on the order of one thousand,[2c,5] see the Supporting Information, Section 1) to affect even small shifts in the nanoparticles' SPR bands.[7] Improving the existing detection limits therefore requires amplification of the assembly/disassembly process. Unfortunately, the repertoire of amplification procedures compatible with nanoparticle-based assays is currently limited to the catalytic deposition of silver on surface-immobilized AuNPs.[8] Herein, we show that NP supracrystals and previously unreported core–shell (CS) supracrystals (Figure 1) stabilized by analyte-specific cross-linkers can enhance dramatically (by over two orders of magnitude compared to noncrystalline NP aggregates) the sensitivity of NP-based detection. The cross-linked crystals are insoluble in water and, owing to NP aggregation, do not exhibit SPR in the visible regime. When, however, an analyte (an anion, a small molecule, or an enzyme) is present, it cuts the cross-linkers so that each crystal liberates, like a pinched "balloon" (Figure 2, Figure 3), millions of individual NPs absorbing strongly in the visible regime and effectively amplifying the molecular-scale "cutting" events into pronounced color changes visible to a naked eye (Figure 4). Moreover, in the CS supracrystals, the "shell" and the "core" regions have different NP compositions and are stabilized with different cross-linkers; consequently, these crystals can dissolve in a step-wise fashion under the action of two different analytes (Figure 5). This property allows for spatially distributed sensing, whereby the crystals release their cargo only if they travel through specific concentration landscapes of the analytes.

We used AuNPs with an approximate diameter of (5.6 ± 0.5) nm and AgNPs of diameter (5.6 ± 1.2) nm coated with self-assembled monolayers (SAMs) of either positively charged *N,N,N*-trimethyl(11-mercaptoundecyl)ammonium chloride ($HS(CH_2)_{11}N(CH_3)_3^+$, TMA, ProChimia, Poland) or negatively charged, deprotonated mercaptoundecanoic acid ($HS(CH_2)_{10}COO^-$, MUA, ProChimia; Figure 1a). The AuNPs had a strong surface plasmon resonance (SPR) band with maximum at $\lambda_{max} = 520$ nm, and their aqueous solutions appeared bright red; for AgNPs, $\lambda_{max} \approx 420$ nm and particle solutions appeared yellow. Supracrystals (henceforth, simply "crystals") were grown by slow evaporation of water from DMSO/water mixtures containing equal numbers of oppositely charged NPs (see Ref. [9] and the Supporting Information, Section 2 for details). The 1–2 μm crystals (Figure 1b) thus assembled (ca. 2.2×10^7 crystals per mL) were held together by electrostatic interactions between the NPs, comprised several million nanoparticles each (ca. 2.5×10^6 NPs as determined by SEM imaging), and were soluble in water. Upon exposure to alkane dithiols that cross-linked the nearby NPs, however, the crystals became stable in water (Figure 2a) and could be used as seeds or cores to epitaxially deposit an additional shell of NPs. These shell NPs were again deposited from an aqueous solution of oppositely charged particles,[10] the material properties of which could be different from those in the crystal core. In this way, core–shell crystals (each up to ca. 2.5 μm across, Figure 1c, shell thickness ca. 200–300 nm, Figure 5) were assembled and could be stabilized and made insoluble in water by additional dithiol cross-links. The presence of the core–shell architecture was confirmed directly by EDX (energy dispersive X-ray spectroscopy) scans of the crystals' composition (Figure 1c and Figure 5) and indirectly by the fact that the shell regions could be dissolved without destroying the crystalline core (see Figure 5). Both the "regular" and the CS crystals slowly (within hours) sedimented from solution and appeared as a dark gray powder.

The crux of the amplified detection (Figure 2a) was to prepare crystals stabilized by dithiols incorporating groups that can be cleaved by desired analytes. We considered three such dithiols (Figure 2b; see the Supporting Information, Section 2 for synthetic details): 11-mercaptoundecyl-11-mercaptoundecanoate (**1**) containing an ester moiety prone to base hydrolysis; 11-mercapto-*N*-(pyridin-2-yl)undecanamide held together by coordination of Cu^{II} to two pyridine and two carbonyl groups (**2**), which cleaves upon addition of a stronger chelating agent such as ethylenediaminetetraacetic acid (EDTA), and *N*-(6-amino-1-(11-mercaptoundecylamino)-1-

[*] Dr. B. Kowalczyk, D. A. Walker, S. Soh, Prof. B. A. Grzybowski
Department of Chemical and Biological Engineering
Northwestern University
2145 Sheridan Rd., Evanston, IL 60208 (USA)
Fax: (+1) 847-491-3728
E-mail: grzybor@northwestern.edu
Homepage: http://dysa.northwestern.edu
Dr. B. Kowalczyk, Prof. B. A. Grzybowski
Department of Chemistry, Northwestern University
2145 Sheridan Rd., Evanston, IL 60208 (USA)

[**] This work was supported by the Non-equilibrium Energy Research Center (NERC), which is an Energy Frontier Research Center funded by the U.S. Department of Energy, Office of Science, Office of Basic Energy Sciences under Award Number DE-SC0000989.

Supporting information for this article is available on the WWW under http://dx.doi.org/10.1002/anie.201002295.

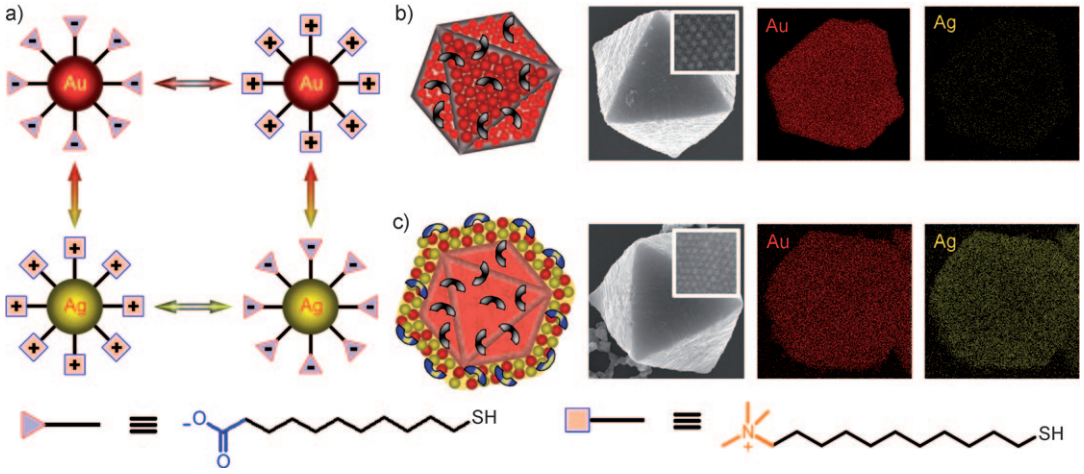

Figure 1. Nanoparticles, crystals, and core–shell crystals. a) Scheme of Au and Ag nanoparticles and of the charged MUA and TMA ligands coating them. Arrows indicate the pairs of oppositely charged NPs that can form supracrystals. b) Scheme of a NP supracrystal (here made of AuTMA and AuMUA NPs); gray-black arcs indicate dithiol cross-links bridging proximal NPs at the crystal's surface. The SEM image shows a typical crystal composed of AuTMA and AuMUA NPs (scale bar = 500 nm); the inset shows individual, ordered NPs on the crystal's surface (scale bar = 20 nm). The two rightmost images have compositional maps of an AuTMA/AuMUA crystal recorded on STEM (scanning transmission electron microscope) equipped with dual Thermo-Scientific EDS (energy dispersive X-ray spectroscopy) detectors (color coding: Au = red; Ag = yellow). These maps confirm that the crystal is composed solely of Au particles. c) A scheme, SEM image, and compositional maps of a core–shell crystal. Here, the core of the crystal is made from AuTMA and AuMUA NPs and is stabilized with cross-linker **3** (gray-black arcs). A mixture of AgTMA and AuMUA NPs is then deposited onto this cross-linked core, and the entire layered structure is stabilized with cross-linker **1** (also see Figure 5).

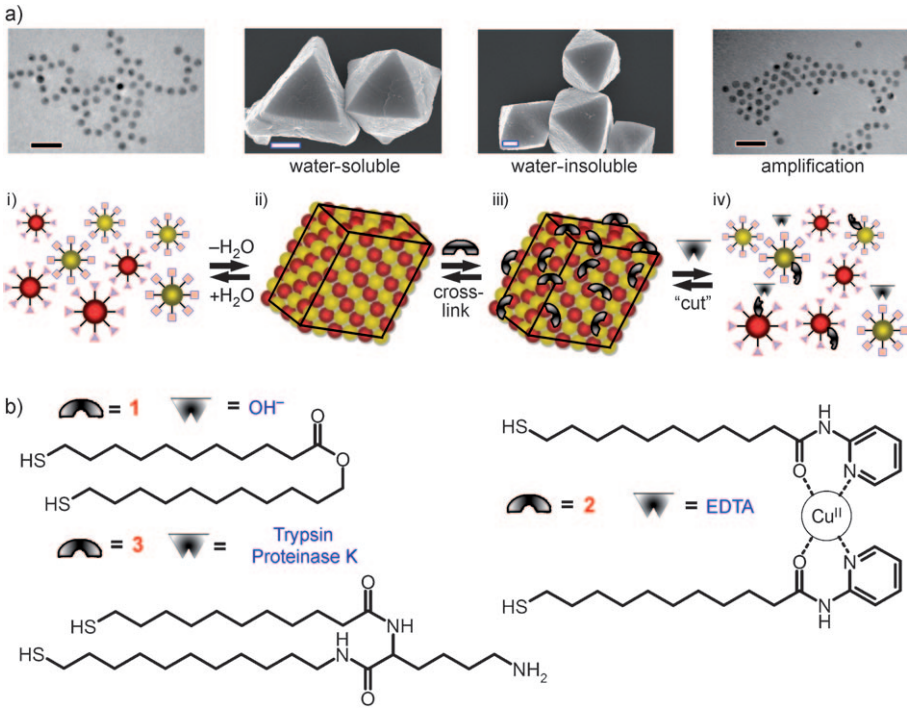

Figure 2. Amplified chemical sensing using nanoparticle supracrystals. a) Crystals, each containing several million NPs, self-assemble from oppositely charged NPs (i) and are soluble in water (ii). These crystals gain permanence and become water-insoluble when they are cross-linked with dithiols containing cleavable groups (iii). When a specific analyte is added, the cross-links are chemically cut, and the crystals disintegrate into individual nanoparticles (iv). Scale bars are 250 nm in the SEM images of crystals and 20 nm in the TEM images of free NPs. b) Chemical structures of the dithiol cross-linkers **1**–**3** and the analytes that cut them.

oxohexan-2-yl)-11-mercaptoundecanamide (**3**), incorporating a lysine amino acid and cleaving in the presence of proteases such as trypsin or proteinase K (but not papain). In all cases, the stability of NP crystals in water increased with increasing dithiol concentration C_{DT} (see Figure S1a in the Supporting Information). On the other hand, if too much dithiol was used, the tightly knit crystals were hard to dissolve upon exposure to dithiol-cutting analytes, and the sensitivity of detection was poor. Consequently, the crystals we used were cross-linked with the minimal concentration of dithiols ($C_{DT}^{min} \approx 2$ mM, 6–8 h soaking) necessary to stabilize these crystals in water such that no individual NPs dissolved in solution could be detected by either UV/Vis spectroscopy, DLS (dynamic light scattering), or TEM (transmission electron microscopy).

Reaction-diffusion modeling accounting for the diffusion of the dithiols into the nanometer-sized[9a] pores of the crystals and for the displacement of the TMA/MUA thiols from the NPs estimates the thickness of the cross-linked layer to

be on the order of $L \approx 15$–30 nm from the crystal's surface (see the Supporting Information, Section 4 for details). In other words, only the "skin" of the crystals is cross-linked, and when it is ruptured, the crystals should liberate large numbers of the interior, un-cross-linked NPs.

This, indeed, is what was observed in experiments. We first discuss the results for the regular (i.e., not CS) crystals. When an analyte specific to the cleavable dithiols was added, the crystals dissolved, thus coloring the solution brightly (Figure 3a). SEM imaging (Figure 3b) indicates that crystals

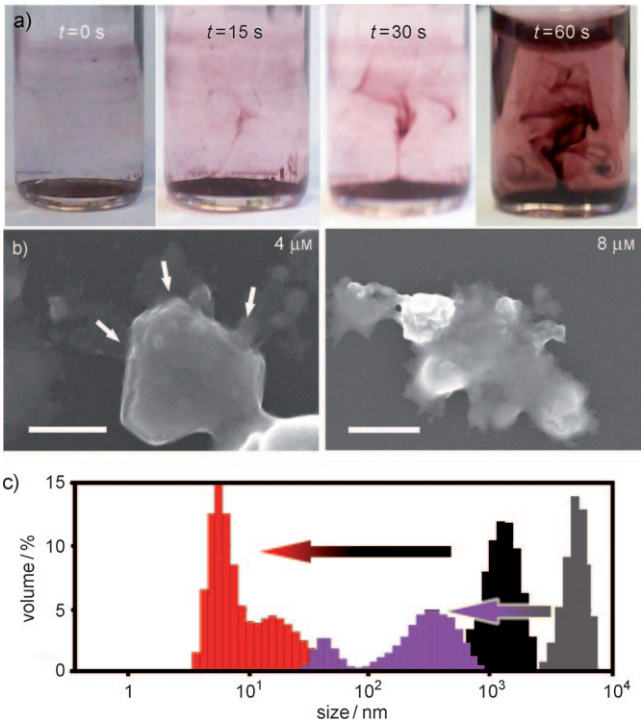

Figure 3. Dissolution of cross-linked crystals. a) Optical images illustrating dissolution of the crystals (here, cross-linked with **1**) upon addition of $(CH_3)_4N^+OH^-$ base (10 mM, 5 μL). b) Gradual dissolution of the crystals from (a) monitored using SEM. The concentrations of the base added are indicated in the upper-right corners of the images. The hazy regions around the crystal in the left image (indicated by white arrows) correspond to individual NPs "spilling out" (see the Supporting Information, Section 3 for high-resolution images). Scale bars = 1 μm. c) Particle size distributions recorded by DLS on a Malvern ZetaSizer Nano-ZS instrument (see the Supporting Information, Section 2.2). Black: undissolved NP crystals cross-linked with **1.** Red: particles from the dissolution of the crystals (upon addition of 10 μL 10 mM $(CH_3)_4N^+OH^-$). Gray: cross-linked, disordered NPs (cross-linker **1**). Violet: aggregates from the dissolution of the disordered aggregates (after 24 h; cutting agent: 10 μL 50 mM $(CH_3)_4N^+OH$).

dissolved from one or few locations on their surfaces. These locations were usually along crystal's edges or near its vertices, where the surface NPs were the least stable (i.e., corresponding to the highest free energies).[11] Once a small hole was "pinched" in the crystal's cross-linked "skin", large numbers of individual NPs spilled from the crystal's interior into the solution. DLS measurements (Figure 3c, black and red histograms) confirmed that this process—even for the lowest analyte concentrations used—gave mostly individual NPs rather than nanoparticle clusters in solution. This behavior was in sharp contrast to that observed in control experiments, where we studied the dissolution of cross-linked but disordered NP aggregates (Figure 3c, violet and gray histograms). Such aggregates not only required a much higher concentration of dithiols to be stable in water ($C_{DT}^{min} \gg 10$ mM) but also dissolved slowly and gradually—first into smaller, colorless aggregates and only then into individual NPs. As a result, the sensitivity of detection was much lower upon the dissolution of disordered aggregates than NP crystals.

These trends are quantified in Figure 4a–c, which plots the solution's absorbance *Abs* (proportional to the concentration of dissolved NPs) as a function of the concentration of the added analyte C_A (here, EDTA cutting cross-links of **2**).

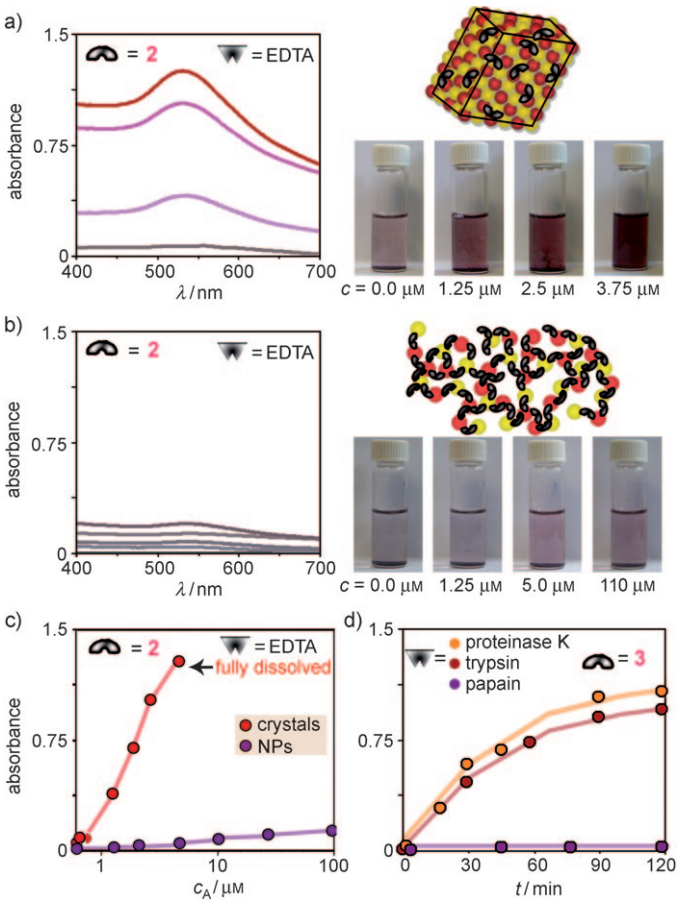

Figure 4. Dissolution of NP crystals and of disordered NP aggregates. a) UV/Vis spectra indicate dissolution of crystals (stabilized by **2**) upon gradual addition of EDTA. The corresponding images in the right column illustrate the changes in the solution color; the red color is due to individual AuNPs from the dissolved crystals. b) Control experiment in which EDTA is added to disordered, cross-linked aggregate. Even for high concentrations of EDTA, only a small fraction of the aggregates dissolves into free NPs, and the solutions are barely colored. c) Comparison of the two experiments quantified by absorbance at $\lambda_{max} \approx 530$ nm. For a given concentration of EDTA, the colorimetric response of the crystals is approximately 100 times stronger than that of disordered aggregates. d) Kinetics of dissolution of crystals cross-linked with **3** upon addition of trypsin (red) and proteinase K (yellow), both at the same 5 μM enzyme concentration, at $T = 37$ °C for trypsin and 50 °C for proteinase K. Crystals are stable against papain (violet), which does not cleave the cross-linker **3**.

For a given value of C_A, *Abs* measured for the crystals was approximately 100 times greater than the absorbance from dissolving disordered aggregates (Figure 4c). In other words, the use of cross-linked crystals offered an approximately two-orders-of-magnitude improvement in sensitivity compared to cross-linked but disordered NPs. The dissolution of crystals was also much more rapid. A typical crystal sample (ca. 8.8×10^7 crystals or 2.2×10^{14} NPs in 4 mL solvent) exposed to an analyte of concentration $C_A\approx1$ μM dissolved completely within 60 s; for a disordered NP aggregate exposed to a tenfold higher analyte concentration, the time to see even a bleak color was on the order of tens of minutes. Lastly, for the crystals, the smallest change in the solution's color discernible to a naked eye ($Abs\approx0.3$–0.4 in a 10 mm cuvette) was 14 EDTA molecules per one AuTMA/MUA nanoparticle. This result compares favorably with conventional NP-based colorimetric methods,[2b,4a,5] which require approximately 1000 or more analyte molecules to effect even minute spectral shifts or changes detectable only using spectroscopic methods. Qualitatively similar trends to those for **2**/EDTA were observed for the dithiol **1**/OH^- analyte pair, for which the smallest visually detectable change corresponded to 43 analyte molecules per NP, and dissolution time was approximately 90 s. In both cases, the crystals were not dissolved by analytes not specific to the dithiol cross-linkers.

Crystals stabilized with dithiols containing enzyme-specific motifs were also used as selective enzymatic sensors. For instance, crystals cross-linked with lysine-containing **3** were dissolved readily by $C_A\approx5$ μM solutions of serine proteases such as trypsin or proteinase K (Figure 4d), the active centers

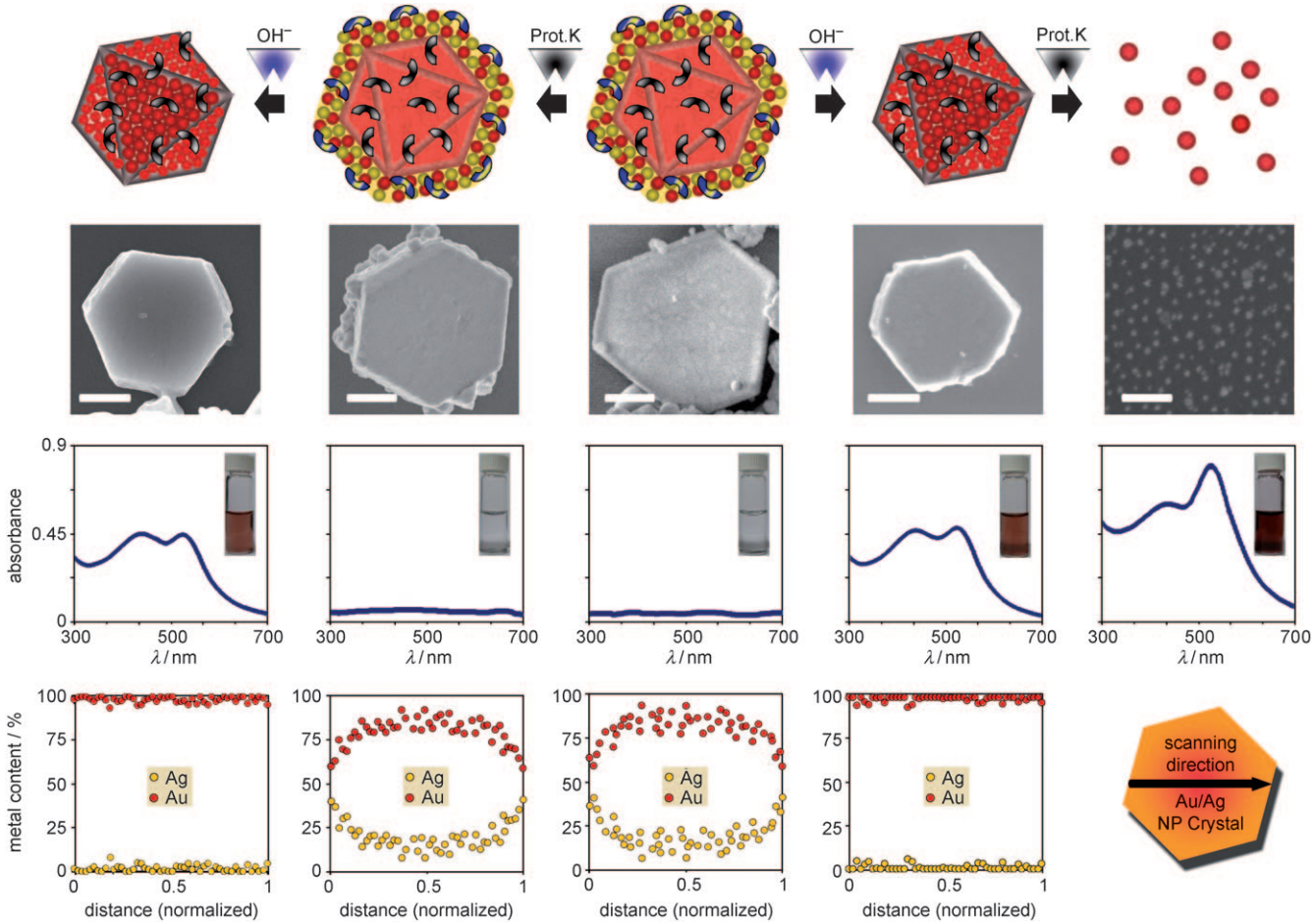

Figure 5. Sensing by core–shell crystals. When the core–shell crystals (middle column) are exposed first to the solution of an analyte cutting the outer cross-links (here OH^- cutting **1**) and are then transferred into the solution containing analytes cutting the inner cross-links (here proteinase K cutting **3**), both the core and the shell dissolve completely into individual NPs (rightmost column). When, however, the crystals are first exposed to the enzyme and only then to the base, only the shell dissolves, thus leaving behind intact crystal "cores" (leftmost column). The specific crystals used here have cores composed of AuTMA and AuMUA NPs and shells made of AgTMA and AuMUA NPs. The second row from the top shows typical SEM images of the crystals (scale bars = 500 nm; 100 nm in the rightmost image). The third row shows the UV/Vis spectra and optical images of the solutions. Solutions are colorless if crystals are not dissolved, orange if only the shells are dissolved, and dark red if both the shells and the cores are dissolved. The bottom row has typical EDS composition scans across individual crystals. Intact core–shell crystals contain $\chi_{Au}\approx78\%$ Au and $\chi_{Ag}\approx22\%$ Ag (composition averaged over scan length); when the shell is dissolved, the composition of the core is pure Au. Note that near the ends of the scan of intact CS crystals, the composition of Ag increases to approximately 50%, as predominantly the crystal's Au/Ag shell is probed by the beam. Shell thickness x_{sh} can be estimated from the elemental composition near the middle of the crystal, $\chi_{Au}\approx85\%$, where the beam passes through two Au/Ag shells (each of thickness x_{sh}; Au metal content 50%) and the Au/Au core (thickness x_{core}; Au content 100%). For 2 μm crystals, the equations $(100\%\,x_{core}+2\,50\%\,x_{sh})/(x_{core}+2x_{sh})=0.85$ and $(x_{core}+2x_{sh})=2$ μm give an estimated $x_{sh}\approx300$ nm.

of which contain the serine-histidine-aspartate catalytic triad.[12a] The smallest change in the solution color detectable by a naked eye corresponded to 56 molecules of trypsin or proteinase K per one liberated nanoparticle. In contrast, the same crystals remained stable in the presence of even high ($C_A > 0.1$ mM) concentrations of the protease papain (violet curve in Figure 4d), whose catalytic triad is cysteine-histidine-asparagine[12b] and which has low affinity to **3**.[12c] Interestingly, the rates of crystal dissolution were similar for trypsin and for proteinase K, despite the fact that the rates of proteolytic cleavage of free **3** by these enzymes are quite different (tens of minutes for trypsin[13a] and a few minutes for proteinase K[13b]). This observation suggests that crystal dissolution is limited by the slow diffusion of large enzymes into the nanoscopic pores of the crystals' cross-linked "skin" layer. This limited accessibility of the cross-linkers' cleavable group can also rationalize why the dissolution of the crystals was markedly slower (15–30 min to reach $Abs \approx 0.3$–0.4) than in the previously discussed **2**/EDTA or **1**/OH^- systems. Still, these times are commensurate with those for commercial proteinase assays (typically, tens of minutes to hours[14]).

The core–shell crystals (see Figure 1c) enable additional modes for amplified sensing, especially when the core and shell regions are made of different NPs and are stabilized by cross-linkers specific to different analytes. Under such conditions, it is possible to dissolve the core and the shell selectively and to liberate the NPs that compose these regions sequentially. While in homogeneous solutions such sequential sensing is probably of little advantage (one can always use two types of "regular" crystals, each stabilized with different cross-links), it can be of use in "stratified" media in which different regions contain different types of analytes. This situation is illustrated in Figure 5 for CS crystals comprising Au cores stabilized with **3** and Au/Ag shells stabilized with **1**. When these crystals are first exposed to a medium containing OH^- analyte (cutting the outer **1** cross-links), the shell dissolves; subsequent passage through a medium containing proteinase K (cutting inner **3** cross-links) dissolves the crystal's core. Importantly, when the same crystals are passed through the same media but in reverse order, only shells dissolve, but the cores remain intact. In other words, the crystals perform spatially distributed sensing, whereby they report the path they traveled (note that this cannot be achieved with mixtures of "regular" crystals of different types stabilized by different cross-linkers). We suggest that this property can be even more relevant to nanoparticle-based delivery systems, whereby appropriately structured and cross-linked CS crystals traveling through chemically stratified media release their cargo sequentially in desired locations.

In summary, nanoparticle crystals of different internal architectures, including unprecedented core–shell NP crystals, and stabilized with chemically cleavable cross-links effectively "amplify" the presence of cross-link-specific analytes into pronounced color changes. This mode of sensing can be generalized to different cross-link/analyte combinations. An exciting opportunity for future research would be to use supracrystals of medically relevant nanoparticles (e.g., antibacterial AgNPs, antifungal CuNPs, anticancer arsenic NPs, MRI contrast-enhancing magnetite NPs) in biodelivery applications, where the crystals, especially the CS ones, could dissolve and liberate their contents sequentially upon reaching specific intracellular targets.

Received: April 18, 2010
Published online: July 13, 2010

Keywords: amplification · nanoparticles · self-assembly · sensors

[1] a) T. A. Taton, C. A. Mirkin, R. L. Letsinger, *Science* **2000**, *289*, 1757; b) C. A. Mirkin, R. L. Letsinger, R. C. Mucic, J. J. Storhoff, *Nature* **1996**, *382*, 607.

[2] a) Y. J. Kim, R. C. Johnson, J. T. Hupp, *Nano Lett.* **2001**, *1*, 165; b) J. W. Liu, Y. Lu, *J. Am. Chem. Soc.* **2003**, *125*, 6642.

[3] a) S. Link, M. A. El-Sayed, *Int. Rev. Phys. Chem.* **2000**, *19*, 409; b) A. O. Pinchuk, A. M. Kalsin, B. Kowalczyk, G. C. Schatz, B. A. Grzybowski, *J. Phys. Chem. C* **2007**, *111*, 11816.

[4] a) R. Chakrabarti, A. M. Klibanov, *J. Am. Chem. Soc.* **2003**, *125*, 12531; b) A. Charrier, N. Candoni, F. Thibaudau, *J. Phys. Chem. B* **2006**, *110*, 12896; c) K. Sato, K. Hosokawa, M. Maeda, *J. Am. Chem. Soc.* **2003**, *125*, 8102.

[5] a) J. H. Lee, Z. D. Wang, J. W. Liu, Y. Lu, *J. Am. Chem. Soc.* **2008**, *130*, 14217; b) J. W. Liu, Y. Lu, *Angew. Chem.* **2006**, *118*, 96; *Angew. Chem. Int. Ed.* **2006**, *45*, 90.

[6] a) J. J. Storhoff, A. D. Lucas, V. Garimella, Y. P. Bao, U. R. Muller, *Nat. Biotechnol.* **2004**, *22*, 883; b) C. S. Thaxton, D. G. Georganopoulou, C. A. Mirkin, *Clin. Chim. Acta* **2006**, *363*, 120.

[7] a) J. N. Anker, W. P. Hall, O. Lyandres, N. C. Shah, J. Zhao, R. P. Van Duyne, *Nat. Mater.* **2008**, *7*, 442; b) C. L. Schofield, A. H. Haines, R. A. Field, D. A. Russell, *Langmuir* **2006**, *22*, 6707.

[8] a) Y. Y. Li, C. Zhang, B. S. Li, L. F. Zhao, X. B. Li, W. J. Yang, S. Q. Xu, *Clin. Chem.* **2007**, *53*, 1061; b) A. Virel, L. Saa, V. Pavlov, *Anal. Chem.* **2009**, *81*, 268.

[9] a) A. M. Kalsin, M. Fialkowski, M. Paszewski, S. K. Smoukov, K. J. M. Bishop, B. A. Grzybowski, *Science* **2006**, *312*, 420; b) B. Kowalczyk, A. M. Kalsin, R. Orlik, K. J. M. Bishop, A. Z. Patashinski, A. Mitus, B. A. Grzybowski, *Chem. Eur. J.* **2009**, *15*, 2032.

[10] We emphasize that cross-linking of the "seed" NP crystals was essential for the deposition of any additional NPs in water; without being cross-linked, the seeds simply dissolved into individual NPs.

[11] a) L. Brecevic, D. Kralj, *Interfacial Dynamics*, CRC, Boca Raton, FL, **2000**, p. 435; b) R. Hacquart, J. Jupille, *Chem. Phys. Lett.* **2007**, *439*, 91; c) R. C. Snyder, M. F. Doherty, *AIChE J.* **2007**, *53*, 1337.

[12] a) P. A. Frey, S. A. Whitt, J. B. Tobin, *Science* **1994**, *264*, 1927; b) T. Vernet, D. C. Tessier, J. Chatellier, C. Plouffe, T. S. Lee, D. Y. Thomas, A. C. Storer, R. Menard, *J. Biol. Chem.* **1995**, *270*, 16645; c) A. Berger, I. Schechter, *Philos. Trans. R. Soc. London Ser. B* **1970**, *257*, 249.

[13] a) J. Lough, D. S. Wrenn, H. M. Miziorko, H. E. Auer, *Int. J. Biochem.* **1985**, *17*, 309; b) W. Ebeling, N. Hennrich, M. Klockow, H. Metz, H. D. Orth, H. Lang, *Eur. J. Biochem.* **1974**, *47*, 91.

[14] Examples of times needed to observe color change in different commercial protease assays include QuantiCleave protease assay kit: within 1 h, protease assay kit from G Biosciences: 2.5 h, EnzChek peptidase/protease assay kit from Invitrogen: 1 h.

